Attenuated replication and pathogenesis of SARS-CoV-2 B.1.1.529 Omicron

Kwok-Yung Yuen (kyyuen@hku.hk)
The University of Hong Kong https://orcid.org/0000-0002-2083-1552

Huiping Shuai
The University of Hong Kong

Jasper Fuk-Woo Chan
The University of Hong Kong https://orcid.org/0000-0001-6336-6657

Bingjie Hu
The University of Hong Kong

Yue Chai
The University of Hong Kong

Terrence Tsz-Tai Yuen
The University of Hong Kong

Xiner Huang
The University of Hong Kong https://orcid.org/0000-0002-0154-8372

Chaemin Yoon
The University of Hong Kong

Jingchu Hu
Shenzhen Institutes of Advanced Technology https://orcid.org/0000-0001-6144-7226

Huan Liu
The University of Hong Kong

Jialu Shu
The University of Hong Kong

Yuanchen Liu
The University of Hong Kong

Tianrenzheng Zhu
The University of Hong Kong

Jinjin Zhang
The University of Hong Kong

Yuxin Hou
The University of Hong Kong

Jian-Piao Cai
The University of Hong Kong

Jinxia Zhang

Department of microbiology https://orcid.org/0000-0002-5087-3614
Jie Zhou
University of Hong Kong https://orcid.org/0000-0002-2948-3873
Feifei Yin
Hainan Medical University
Shuofeng Yuan
The University of Hong Kong
Bao-Zhong Zhang
Shenzhen Institutes of Advanced Technology
Jiandong Huang
The University of Hong Kong https://orcid.org/0000-0001-7531-2816
Hin Chu
The University of Hong Kong https://orcid.org/0000-0003-2855-9837

Biological Sciences - Article

Keywords:

Posted Date: December 29th, 2021

DOI: https://doi.org/10.21203/rs.3.rs-1200124/v1

Version of Record: A version of this preprint was published at Nature on January 21st, 2022. See the published version at https://doi.org/10.1038/s41586-022-04442-5.

Title: Attenuated replication and pathogenesis of SARS-CoV-2 B.1.1.529 Omicron

Authors:

Huiping Shuai[1,*], Jasper Fuk-Woo Chan[1,2,3,4,5,6,*], Bingjie Hu[1,*], Yue Chai[1,*], Terrence Tsz-Tai Yuen[1,*], Xiner Huang[1], Chaemin Yoon[1], Jing-Chu Hu[7], Huan Liu[1], Jialu Shi[1], Yuanchen Liu[1], Tianrenzheng Zhu[1], Jinjin Zhang[1], Yuxin Hou[1], Jian-Piao Cai[1], Anna Jinxia Zhang[1,3], Jie Zhou[1], Feifei Yin[5,6,8], Shuofeng Yuan[1,2,3], Bao-Zhong Zhang[7], Jian-Dong Huang[9], Kelvin Kai-Wang To[1,2,3,4], Kwok-Yung Yuen[1,2,3,4,5,6,#], Hin Chu[1,2,3,#]

Affiliations:

[1]State Key Laboratory of Emerging Infectious Diseases, Department of Microbiology, and Carol Yu Centre for Infection, Li Ka Shing Faculty of Medicine, The University of Hong Kong; Pokfulam, Hong Kong Special Administrative Region, People's Republic of China.

[2]Department of Clinical Microbiology and Infection Control, The University of Hong Kong-Shenzhen Hospital; Shenzhen, Guangdong, People's Republic of China.

[3]Centre for Virology, Vaccinology and Therapeutics; Hong Kong Science and Technology Park, Hong Kong Special Administrative Region, People's Republic of China.

[4]Department of Microbiology, Queen Mary Hospital; Pokfulam, Hong Kong Special Administrative Region, People's Republic of China.

[5]Hainan Medical University-The University of Hong Kong Joint Laboratory of Tropical Infectious Diseases, The University of Hong Kong; Pokfulam, Hong Kong Special Administrative Region, China.

[6]Academician Workstation of Hainan Province, Hainan Medical University; Haikou, Hainan, People's Republic of China.

[7]CAS Key Laboratory of Quantitative Engineering Biology, Shenzhen Institute of Synthetic Biology, Shenzhen Institutes of Advanced Technology, Chinese Academy of Sciences; Shenzhen, People's Republic of China.

[8]Key Laboratory of Tropical Translational Medicine of Ministry of Education, Hainan Medical University; Haikou, Hainan, China.

[9]School of Biomedical Sciences, Li Ka Shing Faculty of Medicine, The University of Hong Kong; Pokfulam, Hong Kong Special Administrative Region, People's Republic of China.

*These authors contributed equally to this work

#Corresponding author. Email: Hin Chu (hinchu@hku.hk) and Kwok-Yung Yuen (kyyuen@hku.hk)

Summary

SARS-CoV-2 Omicron emerged in November 2021 and is rapidly spreading among the human populations. The variant contains 34 changes in its spike protein including 15 substitutions at the receptor-binding domain (RBD). While recent reports reveal that the Omicron variant can robustly escape from vaccine and therapeutic neutralization antibodies, the pathogenicity of the virus remains unknown. Here, we investigate the virological features and pathogenesis of the Omicron variant using in vitro and in vivo models. Our results demonstrate that the replication of the Omicron variant is dramatically attenuated in Calu3 and Caco2 but not in VeroE6 cells. Further mechanistic investigations reveal that the Omicron variant is deficient in transmembrane serine protease 2 (TMPRSS2) usage in comparison to that of WT, Alpha, Beta, and Delta variant, which explained its inefficient replication in Calu3 and Caco2 cells. Importantly, the replication of the Omicron variant is markedly attenuated in both the upper and lower respiratory tract of infected K18-hACE2 mice in comparison to that of WT and Delta variant, which results in its dramatically ameliorated lung pathology. When compared with SARS-CoV-2 WT, Alpha, Beta, and Delta variant, infection by the Omicron variant causes the least body weight loss and mortality rate. Overall, our study demonstrates that the Omicron variant is significantly attenuated in virus replication and pathogenicity in comparison with WT and previous variants. Our data suggest the current global vaccination strategy has forced SARS-CoV-2 into a new evolutionary trajectory towards reduced replication fitness in exchange of better immune escape. These findings are critical for setting policy in the pandemic control and disease management of COVID-19.

Main Text:

Coronavirus Disease 2019 (COVID-19) is caused by severe acute respiratory syndrome coronavirus 2 (SARS-CoV-2)[1,2]. Since its emergence in 2019, SARS-CoV-2 continues to evolve by acquiring mutations that increase transmissibility, modulate pathogenicity, or confer resistance to neutralization antibodies. A new SARS-CoV-2 variant (PANGO lineage B.1.1.529) was reported on 24 November 2021 from Botswana and South Africa. Within 2 days, the World Health Organization (WHO) Technical Advisory Group classified B.1.1.529 as the fifth variant of concern (VOC), and designated it as the Omicron variant.

The Omicron variant is characterized by an unusually large amount of mutations at the spike protein, including 30 amino acid substitutions, three deletions, and one insertion, compared with the original SARS-CoV-2. Among these changes, 15 of the amino acid substitutions are located in the receptor-binding domain (RBD) and 3 amino acid substitutions are located at the furin-like cleavage site at the S_1/S_2 junction that may modulate host protease cleavage by furin and transmembrane serine proteases. The abundant mutations at these regions hinted that the Omicron variant may escape from neutralizing antibody in convalescent or vaccinated sera, and modify its capacity in cell entry, replication, and pathogenesis.

Preliminary reports suggest that the Omicron variant is highly transmissible, even in fully vaccinated individuals and individuals that received a booster dose[3-5]. These results are congruous with recent findings that the Omicron variant is markedly resistant to neutralization by sera not only from convalescent patients, but also from individuals vaccinated with many widely used COVID-19 vaccines[6-11]. In addition, the neutralization capacity of monoclonal antibodies (mAbs) in clinical use against COVID-19 is abolished or severely impaired against

the Omicron variant[12-14]. In this regard, the Omicron variant represents a critical threat to the pandemic control and disease treatment of the COVID-19 pandemic.

The number of infection caused by the Omicron variant is growing rapidly with a propensity to replace the Delta variant as the predominant circulating SARS-CoV-2 variant. In contrast to its capacity of escaping antibody neutralization, whether or not the Omicron variant can cause milder or more severe disease remain unknown. In this study, we evaluated the virological features and pathogenesis of the Omicron variant in vitro and in vivo, and compared the results with that of SARS-CoV-2 wildtype (WT) and other VOCs. Our results demonstrate that the replication capacity of the Omicron variant is significantly attenuated both in vitro and in vivo compared with SARS-CoV-2 WT and VOCs, which is explained by the lowered efficiency of its transmembrane serine protease 2 (TMPRSS2) usage. In the K18-hACE2 mouse model, the Omicron variant replicated significantly less efficiently than SARS-CoV-2 WT and Delta variant in both nasal turbinate and lung, and induced substantially attenuated lung pathology. Finally, by comparing body weight loss and survival, our results suggest that the Omicron variant is significantly attenuated when compared with SARS-CoV-2 WT and previous VOCs including Alpha, Beta, and Delta.

Attenuated replication of the Omicron variant

The Delta variant replaced all VOC and was the predominant circulating SARS-CoV-2 variant since mid-2021 **(Fig. 1a)**. Infection caused by the Omicron variant is increasing rapidly since late November 2021, which may become the next predominant circulating SARS-CoV-2 variant **(Fig. 1a)**. We first compared the replication efficiency of the Omicron variant with that of SARS-CoV-2 WT, Alpha, Beta, and Delta variants. We included Omicron (R346K) in the comparison, which contains a R346K mutation in the spike protein that represents 8.5%

(956/11242) of the total Omicron variant sequences deposited into GISAID database as of 19th December 2021. By measuring the subgenomic envelope (sgE) gene that represents replication intermediates, our results suggested that the replication of the Omicron variant was severely attenuated in the Calu3 human lung epithelial cells. Area under the curve (AUC) quantification of the sgE gene generated over a period of 48 hours suggested that Omicron and Omicron (R346K) replicated 3.4- and 4.2-fold less efficiently comparing to SARS-CoV-2 WT **(Fig. 1b)**. In contrast, the Alpha, Beta, and Delta variants replicated to similar or higher levels in comparison to SARS-CoV-2 WT in Calu3 cells **(Fig. 1b)**. We next measured the amount of infectious virus particles produced from SARS-CoV-2 WT- and variants-infected Calu3 cells. In keeping with the sgE gene results, we demonstrated that while Alpha, Beta, and Delta variants produced similar or higher levels of infectious virus particles between 8-48 hours post infection (hpi), the Omicron variant produced significantly less infectious virus particles than that of SARS-CoV-2 WT from Calu3 cells **(Fig. 1c)**. At 48 hpi, the infectious virus titers of Omicron and Omicron (R346K) were 501.4-fold (p=0.0163) and 114.7-fold (p=0.0168) lower than that of SARS-CoV-2 WT, respectively **(Fig. 1c)**. In parallel, we evaluated the replication of the Omicron variant in Caco2 human intestinal epithelial cells. Similar to the results from Calu3 cells, the replication of the Omicron variant was dramatically lower in comparison with that of SARS-CoV-2 WT, Alpha, Beta, and Delta variants **(Extended Data Fig. 1a)**. At 48 hpi, the infectious virus titers of Omicron and Omicron (R346K) were 407.2-fold (p=0.0123) and 238.1-fold (p=0.0124) lower than that of SARS-CoV-2 WT, respectively **(Fig. 1d)**. Interestingly, in VeroE6 cells, the replication of the Omicron variant was only modestly lowered in comparison to that of SARS-CoV-2 WT, and was at a comparable level to the Delta variant **(Fig. 1e and Extended Data Fig. 1b)**. Next, we evaluated the cytopathic effect of the Omicron variant in

VeroE6-TMPRSS2 cells. Our results demonstrated that both Omicron and Omicron (R346K) variant were less cytopathic than SARS-CoV-2 WT as evidenced by the significantly higher cell viability between 12-36 hpi **(Fig. 1f)**. Overall, these findings indicate that the omicron variant replicates less efficiently than SARS-CoV-2 WT, Alpha, Beta, and Delta variants, and induces a comparatively lower level of cell damage in the infected cells.

Mechanism of the attenuated replication of the Omicron variant

Our live virus infection assays demonstrate that the replication of Omicron variant is markedly attenuated in Calu3 and Caco2 cells in comparison to SARS-CoV-2 WT and other variants, while in VeroE6 cells, the replication of Omicron variant is only modestly lowered. Our results are in line with a recent preprint that showed a decrease in pseudovirus entry of the Omicron variant in Calu3 and Caco2 cells but not Vero, 293T, or A549-ACE2 cells[15]. Previous reports have demonstrated that SARS-CoV-2 enters Calu3 and Caco2 cells through the plasma membrane entry pathway mediated by TMPRSS2, while the virus enters TMPRSS2-deficient cells (Vero, VeroE6, 293T, A549) through the endocytic pathway mediated by cathepsin L or other endosomal proteases[16-18]. Combining previous knowledge and current evidence from us and others, we postulate that the spike mutations of the Omicron variant might result in a reduced capacity in TMPRSS2 usage, which severely impaired their entry and replication in Calu3 and Caco2 but not in VeroE6 cells. To evaluate this possibility, we side-by-side assessed the entry of pseudovirus carrying the spike protein of SARS-CoV-2 WT, Alpha, Beta, Delta, or Omicron variant, in 293T cells transfected with ACE2 with or without additional TMPRSS2 overexpression. Our result demonstrated that TMPRSS2 overexpression increased SARS-CoV-2 WT, Alpha, Beta, and Delta pseudovirus entry in 293T-ACE2 cells by 11.3-, 12.6-, 11.7-, and 16-folds, respectively **(Fig. 2a)**. In comparison, TMPRSS2 overexpression increased Omicron

pseudovirus entry by only 4.3-folds, which was significantly lower than that of SARS-CoV-2 WT or other variants ($p<0.0001$) **(Fig. 2a)**. To further validate this result, we side-by-side compared pseudovirus entry in VeroE6 and VeroE6-TMPRSS2 cells. Our results demonstrated that TMPRSS2 expression in the VeroE6-TMPRSS2 stable cell-line increased pseudovirus entry for SARS-CoV-2 WT, Alpha, Beta, and Delta variant by 16.1- ($p<0.0001$), 7.9- ($p=0.0005$), 32.1- ($p<0.0001$), and 48.7-folds ($p<0.0001$), respectively. In contrast, the Omicron pseudovirus was largely insensitive to TMPRSS2 expression and its entry was marginally increased by only 1.3-fold (p=ns) in VeroE6-TMPRSS2 cells when compared to VeroE6 cells **(Fig. 2b)**. Next, we evaluated pseudovirus entry on VeroE6-TMPRSS2 cells in the presence of camostat, a potent TMPRSS2 inhibitor. Our data showed that the inhibitory effect of camostat on Omicron pseudovirus entry was significantly reduced in comparison to that of WT, Alpha, Beta, or Delta pseudovirus (**Fig. 2c**). In line with this result, camostat was similarly less potent in inhibiting the virus replication of Omicron and Omicron (R346K) comparing to WT and other variants in VeroE6-TMPRSS2 cells (**Fig. 2d**). Collectively, our results indicate that the reduced replication capacity of the Omicron variant in cells that use the plasma membrane entry pathway, including Calu3, Caco2, and VeroE6-TMPRSS2, is caused by its reduced efficiency in TMPRSS2 usage.

Attenuated replication and pathogenesis of the Omicron variant in vivo

To explore whether the Omicron variant is also attenuated in vivo, we first compared virus propagation of the Omicron variant to SARS-CoV-2 WT and Delta variant in the K18-hACE2 transgenic mice. 6- to 8-week-old mice were intranasally challenged with SARS-CoV-2 WT, Delta, or Omicron variant, and their tissues were collected for virological assessment. Our results demonstrated that the infection of WT SARS-CoV-2 was very robust along the respiratory tract of the hACE2 transgenic mice as evidenced by the high RdRp gene copy

numbers while Delta variant propagated to a largely comparable level (**Fig. 3a**). In stark contrast, the viral RdRp gene copies in the nasal turbinate of mice challenged with the Omicron variant was markedly reduced by 1138- ($p=0.0324$) and 1821-folds ($p=0.001$) compared to those with WT and Delta variant at 2 dpi, respectively (**Fig. 3a**), despite the same inoculation titers were used for virus challenge among the aforementioned variants. At 4 dpi, the viral gene copies in the Omicron-infected mouse nasal turbinate were reduced by approximately 10-folds compared to mice infected with WT or Delta variant. Similarly, the RdRp gene copies were also significantly lower in the lung of the Omicron variant-infected mice in comparison with their counterparts challenged with WT or Delta variant (**Fig. 3a**).

To understand whether the reduction of viral gene production was due to attenuated virus replication, we quantified the sgRNA of the SARS-CoV-2 E gene. Our results showed that the subgenomic E gene in the nasal turbinate of the Omicron variant-infected mice was significantly lower than that of WT and Delta variant at both 2 and 4 dpi. In particular, at 2 dpi, the sgRNA level was diminished by 442- ($p=0.0129$) and 1450-folds ($p<0.0001$) compared to mice infected with WT and Delta variant, respectively (**Fig. 3b**). Consistently, sgRNA synthesis was also lower in the lung of Omicron-infected mice when compared with those infected with WT or Delta variant, although to a lesser extent than nasal turbinate (**Fig. 3b**). In keeping with the RdRp and subgenomic E gene results, the infectious virus titer in both nasal turbinate and lung of Omicron variant-infected mice was significantly lower than that of the WT-infected mice (**Fig. 3c**). Intriguingly, the infectious virus titer at the nasal turbinate of Omicron variant-infected mice was 48-fold ($p=0.0476$) lower than that of the Delta variant, suggesting less infectious virus shedding from the Omicron-infected nasopharynx than that by the Delta variant (**Fig. 3c**). Since the Omicron variant also carries the N501Y mutation, which allows the infection of wildtype

mice and rats as we and others previously reported [19], we additionally side-by-side characterized the replication of the N501Y-carrying Alpha and Omicron variant in wildtype C57B6 mice. Consistent with the findings in hACE2 transgenic mice, the replication of the Omicron variant in nasal turbinate and lung of wildtype C57B6 mice was significantly attenuated when compared with that of WT and Delta variant (**Extended Data Fig. 2**). In parallel with the virological assessments, we quantified the gene expression of IP-10 and IFNγ, which are hallmark proinflammatory cytokines induced by SARS-CoV-2 infection. We found that the transcription level of IP-10 and IFNγ in both nasal turbinate and lung of Omicron variant-infected mice were significantly down-regulated when compared to those challenged with WT and Delta variant, which represented an alleviated proinflammatory response during the infection by the Omicron variant (**Fig. 3d**).

Next, we investigated the infection outcome of the Omicron variant in comparison to SARS-CoV-2 WT, Alpha, Beta, and Delta variant in K18-hACE2 mice. Our results showed that when compared to WT and previously emerged variants, the body weight loss of mice infected by Omicron variant was significantly milder with onset time at a later stage during the course of infection (**Fig. 3e**). Interestingly, when comparing all variants with WT, we observed a tendency of milder body weight loss in the order of Alpha, Beta, Delta, and Omicron, with Omicron being the mildest (**Extended Data Fig. 3**). Importantly, we took advantage of the K18-hACE2 infection model and compared animal survival upon infection with SARS-CoV-2 WT and variants. Under the same inoculum, mouse survival was lowest for the Alpha variant (0%), followed by WT (20%), Beta (33%), Delta (44%), and was highest for the Omicron variant (57%) (**Fig. 3f**). Statistically, mouse survival for Omicron was significantly higher than Alpha ($p=0.0002$) and WT ($p=0.0377$), but did not reach significance for Beta and Delta. Nevertheless,

the trend of mouse survival was in keeping with results of body weight loss, which demonstrated a propensity of better survival in the order of Alpha, WT, Beta, Delta, and Omicron (**Fig. 3f**).

To evaluate the pathogenicity of Omicron infection in the respiratory tract, we carried out histopathological analysis of the lung tissue of infected hACE2 transgenic mice. In corroboration with findings in the virological assessment, multi-focal expression of the viral nucleocapsid (N) protein was frequently detected in both WT and Delta variant-infected mice, but not in those challenged with the Omicron variant at 2 dpi (**Fig. 4a and Extended Data Fig. 4**). At 4 dpi, abundant N protein continued to accumulate in the alveoli of mice infected with WT and Delta variant. However, only a small amount of N protein expression was sparsely detected in the lung of mice infected with the Omicron variant (**Fig. 4a and Extended Data Fig. 4**). Histological examination of both WT- and Delta variant-infected mouse lungs revealed prominent pathological changes in the alveoli, including collapse of the alveoli wall, proteinaceous exudation in the alveoli cavity, and epithelial damage in the small bronchioles, while interstitial congestion was commonly observed, most likely contributed by infiltrations of inflammatory cells and mononuclear lymphocytes (**Fig. 4b and Extended Data Fig. 5**). In sharp contrast, histopathological changes in the lung of mice infected with the Omicron variant was not evident at 2 dpi. At 4 dpi, localized inflammatory infiltrations leading to thickening of the alveoli septa could be scarcely detected (**Fig. 4b and Extended Data Fig. 5**). Together, our results indicate that the Omicron variant replicates inefficiently in lung cells due to reduced TMPRSS2 usage. The reduced replication capacity of the Omicron variant results in attenuated lung pathology, milder body weight loss, and improved animal survival in vivo.

Discussion

SARS-CoV-2 Omicron that emerged in November 2021 disseminates quickly and may replace Delta as the dominant circulating SARS-CoV-2 variant. Current reports from epidemiology and experimental studies suggest that the Omicron variant can efficiently infect individuals after two-dose of vaccination or even after receiving the third booster dose, due to its strong capacity of evading antibody neutralization[6-11]. Additional reports have demonstrated that the neutralization capacity of therapeutic monoclonal antibodies against the Omicron variant are also severely impaired, including some with completely abolished activity[12-14]. In this regard, understanding the pathogenesis of the Omicron variant will be critical for the prevention, control, and disease treatment of this ongoing COVID-19 pandemic.

In this study, we investigated the virological features and pathogenicity of the Omicron variant using in vitro and in vivo models. Our results demonstrate that the replication of the Omicron variant is dramatically attenuated in Calu3 and Caco2 but not in VeroE6 cells. Further mechanistic investigations reveal that the Omicron variant is deficient in TMPRSS2 usage in comparison to that of WT, Alpha, Beta, and Delta variant, which explained its inefficient replication in Calu3 and Caco2 cells. In keeping with the in vitro results, the replication of the Omicron variant is attenuated in both the upper and lower respiratory tract of infected K18-hACE2 mice in comparison to that of WT and Delta variant, which results in its dramatically ameliorated lung pathology. Most importantly, when compared with SARS-CoV-2 WT, Alpha, Beta, and Delta variant, infection by the Omicron variant triggers the mildest body weight loss with the best animal survival rate. Overall, our study demonstrates that the Omicron variant is significantly attenuated in virus replication and pathogenicity in comparison with WT and other variants, revealing a new evolutionary trajectory of SARS-CoV-2.

The exact change on the Omicron variant that results in the severely impaired replication in Calu3 human lung epithelial cells and the respiratory tract of mice is currently unknown. Interestingly, our live virus infection assays demonstrate that while the replication of Omicron variant is dramatically attenuated in Calu3 and Caco2 cells, it is less affected in VeroE6 cells. Our results are in agreement with a recent preprint that suggested a decreased Omicron-spike pseudovirus entry in Calu3 and Caco2 cells but not in Vero, 293T, or A549-ACE2 cells[15]. Mechanistically, we further demonstrate that Omicron-pseudovirus does not utilize TMPRSS2 for entry as efficiently as SARS-CoV-2-WT-, Alpha-, Beta-, or Delta-pseudoviruses. At the same time, the inhibitory effect on Omicron entry and replication in VeroE6-TMPRSS2 cells by the TMPRSS2 inhibitor, camostat, is significantly weakened in comparison to that of WT or other variants. Thus, our results suggest that the attenuated replication of the Omicron variant in lung cells is due to a reduced efficiency in TMPRSS2 usage by mutations in the spike protein. SARS-CoV-2 spike contains a PRRA insertion at the S_1/S_2 junction that creates a multi-basic furin-like cleavage site. This motif is absent from the spike of SARS-CoV-1, SARS-CoV-related coronaviruses (SARSr-CoVs), or the closely related bat coronavirus RaTG13[20]. Recent reports suggest that this acquired furin-like cleavage site facilitates TMPRSS2 usage[21-23] and is critical for the highly efficient infection of human lung cells and transmission of SARS-CoV-2[16,24,25]. Importantly, the spike of the Omicron variant contains three mutations at or near this furin-like cleavage site, including H655Y, N679K, and P681H, that may modulate TMPRSS2 usage. Since P681H is present in the Alpha variant and H655Y is present in the Gamma variant, the change at these two sites alone is unlikely to have resulted in the reduced TMPRSS2 usage. However, the role of N679K as well as the role of combined changes involving H655Y, N679K, and P681H in association with TMPRSS2 usage should be further investigated.

A large body of timely reports has revealed that the Omicron variant can robustly escape from neutralization antibodies, allowing it to infect fully vaccinated or even booster vaccinated individuals[3,4,6-14]. Our results in this study suggest that the virus replication fitness of the Omicron variant is severely compromised as a trade-off of escaping from neutralization antibodies. SARS-CoV-2 variants emerged prior to Omicron in general acquired mutations in spike that allows better virus propagation in the human respiratory tract and more efficient transmission[26-28]. However, with the current high ratio of global COVID-19 vaccination, we showed that SARS-CoV-2 is evolving into a new direction, focusing more on immune escape rather than further increase of virus replication efficiency. By side-by-side comparing the pathogenicity of SARS-CoV-2 WT, Alpha, Beta, Delta, and Omicron variants in the K18-hACE2 model, we observed an attenuating trend for the emerging variants with the Omicron variant being the mildest. The low pathogenicity in mouse lung infected with the Omicron variant hinted that patients infected with the Omicron variant might develop milder respiratory symptoms in comparison to that of the previous variants.

Our study has limitations including the use of the K18-hACE2 mouse model for pathogenesis studies instead of the primate models that are more similar to humans. However, K18-hACE2 mouse model is a well-established model for SARS-CoV-2 study that allows survival measurement. Using this lethal model, we are able to side-by-side compare the pathogenicity of SARS-CoV-2 WT, Omicron, and other variants in a quantitative manner, which is not possible by using other non-human primate, hamster, or ferret models.

Our study has a number of implications. First, we show that the Omicron variant is severely impaired in virus replication in human lung cells as well as in the respiratory tract of infected animals, suggesting that the rapidly increasing Omicron infections in the human

population is not due to an increase in virus replication fitness but rather due to its robust neutralization antibody evasion. Second, we show that the impaired replication of the Omicron variant results from its decreased capacity of utilizing TMPRSS2. In this regard, our results suggest that therapeutics targeting TMPRSS2 may be less effective against the Omicron variant. Third, our data show that the current global vaccination strategy has forced the virus into a new evolutionary trajectory towards reduced replication fitness in exchange of better immune escape. In this direction, an additional booster dose may drive further attenuation of the virus. Overall, our study reveal key features of the Omicron variant that provide critical information for the prevention, control, and treatment of the current COVID-19 pandemic.

References

1 Zhou, P. *et al.* A pneumonia outbreak associated with a new coronavirus of probable bat origin. *Nature* **579**, 270-273, doi:10.1038/s41586-020-2012-7 (2020).

2 Chan, J. F. *et al.* A familial cluster of pneumonia associated with the 2019 novel coronavirus indicating person-to-person transmission: a study of a family cluster. *Lancet* **395**, 514-523, doi:10.1016/S0140-6736(20)30154-9 (2020).

3 Espenhain, L. *et al.* Epidemiological characterisation of the first 785 SARS-CoV-2 Omicron variant cases in Denmark, December 2021. *Euro Surveill* **26**, doi:10.2807/1560-7917.ES.2021.26.50.2101146 (2021).

4 Brandal, L. T. *et al.* Outbreak caused by the SARS-CoV-2 Omicron variant in Norway, November to December 2021. *Euro Surveill* **26**, doi:10.2807/1560-7917.ES.2021.26.50.2101147 (2021).

5 Team, C. C.-R. SARS-CoV-2 B.1.1.529 (Omicron) Variant - United States, December 1-8, 2021. *MMWR Morb Mortal Wkly Rep* **70**, 1731-1734, doi:10.15585/mmwr.mm7050e1 (2021).

6 Cele, S., Jackson, L., Khan, K., Khoury, D. & Sigal, A. SARS-CoV-2 Omicron has extensive but incomplete escape of Pfizer BNT162b2 elicited neutralization and requires ACE2 for infection. *medRxiv*, doi:10.1101/2021.12.08.21267417 (2021).

7 Wang, Y. *et al.* The significant immune escape of pseudotyped SARS-CoV-2 variant Omicron. *Emerg Microbes Infect* **11**, 1-5, doi:10.1080/22221751.2021.2017757 (2022).

8 Lu, L. *et al.* Neutralization of SARS-CoV-2 Omicron variant by sera from BNT162b2 or Coronavac vaccine recipients. *Clin Infect Dis*, doi:10.1093/cid/ciab1041 (2021).

9 Dejnirattisai, W. *et al.* Reduced neutralisation of SARS-COV-2 Omicron-B.1.1.529 variant by postimmunisation serum. *bioRxiv*, doi:10.1101/2021.12.10.21267534 (2021).

10 Edara, V. *et al.* mRNA-1273 and BNT162b2 mRNA vaccines have reduced neutralizing activity against the SARS-CoV-2 Omicron variant. *bioRxiv*, doi:10.1101/2021.12.20.473557 (2021).
11 Ai, J. *et al.* Omicron variant showed lower neutralizing sensitivity than other SARS-CoV-2 variants to immune sera elicited by vaccines after boost. *Emerg Microbes Infect*, doi:10.1080/22221751.2021.2022440 (2021).
12 Cao, Y. R. *et al.* Omicron escapes the majority of existing SARS-CoV-2 neutralizing antibodies. *bioRxiv*, doi:10.1101/2021.12.07.470392 (2021).
13 Liu, L., Iketani, S., Guo, Y., Chan, J. F. & Ho, D. D. Striking Antibody Evasion Manifested by the Omicron Variant of SARS-CoV-2. *bioRxiv* (2021).
14 VanBlargan, L. A., Errico, J. M., Halfmann, P., Zost, S. J. & Diamond, M. S. An infectious SARS-CoV-2 B.1.1.529 Omicron virus escapes neutralization by several therapeutic monoclonal antibodies. *bioRxiv* (2021).
15 Hoffmann, M. *et al.* The Omicron variant is highly resistant against antibody-mediated neutralization - implications for control of the COVID-19 pandemic. *bioRxiv* (2021).
16 Hoffmann, M., Kleine-Weber, H. & Pöhlmann, S. A Multibasic Cleavage Site in the Spike Protein of SARS-CoV-2 Is Essential for Infection of Human Lung Cells. *Molecular cell* **78**, 779-784.e775, doi:10.1016/j.molcel.2020.04.022 (2020).
17 Koch, J. *et al.* TMPRSS2 expression dictates the entry route used by SARS-CoV-2 to infect host cells. *The EMBO journal* **40**, e107821, doi:10.15252/embj.2021107821 (2021).
18 Beumer, J. *et al.* A CRISPR/Cas9 genetically engineered organoid biobank reveals essential host factors for coronaviruses. *Nat Commun* **12**, 5498, doi:10.1038/s41467-021-25729-7 (2021).
19 Shuai, H. *et al.* Emerging SARS-CoV-2 variants expand species tropism to murines. *EBioMedicine* **73**, 103643, doi:10.1016/j.ebiom.2021.103643 (2021).
20 Coutard, B. *et al.* The spike glycoprotein of the new coronavirus 2019-nCoV contains a furin-like cleavage site absent in CoV of the same clade. *Antiviral research* **176**, 104742, doi:10.1016/j.antiviral.2020.104742 (2020).
21 Mykytyn, A. Z. *et al.* SARS-CoV-2 entry into human airway organoids is serine protease-mediated and facilitated by the multibasic cleavage site. *eLife* **10**, doi:10.7554/eLife.64508 (2021).
22 Lamers, M. M. *et al.* Human airway cells prevent SARS-CoV-2 multibasic cleavage site cell culture adaptation. *eLife* **10**, doi:10.7554/eLife.66815 (2021).
23 Laporte, M. *et al.* The SARS-CoV-2 and other human coronavirus spike proteins are fine-tuned towards temperature and proteases of the human airways. *PLoS pathogens* **17**, e1009500, doi:10.1371/journal.ppat.1009500 (2021).
24 Chu, H. *et al.* Host and viral determinants for efficient SARS-CoV-2 infection of the human lung. *Nat Commun* **12**, 134, doi:10.1038/s41467-020-20457-w (2021).
25 Peacock, T. P. *et al.* The furin cleavage site in the SARS-CoV-2 spike protein is required for transmission in ferrets. *Nature microbiology* **6**, 899-909, doi:10.1038/s41564-021-00908-w (2021).
26 Mlcochova, P. *et al.* SARS-CoV-2 B.1.617.2 Delta variant replication and immune evasion. *Nature* **599**, 114-119, doi:10.1038/s41586-021-03944-y (2021).
27 Liu, Y. *et al.* Delta spike P681R mutation enhances SARS-CoV-2 fitness over Alpha variant *bioRxiv* (2021).

28 Saito, A. *et al.* Enhanced fusogenicity and pathogenicity of SARS-CoV-2 Delta P681R mutation. *Nature*, doi:10.1038/s41586-021-04266-9 (2021).

Figures and figure legends

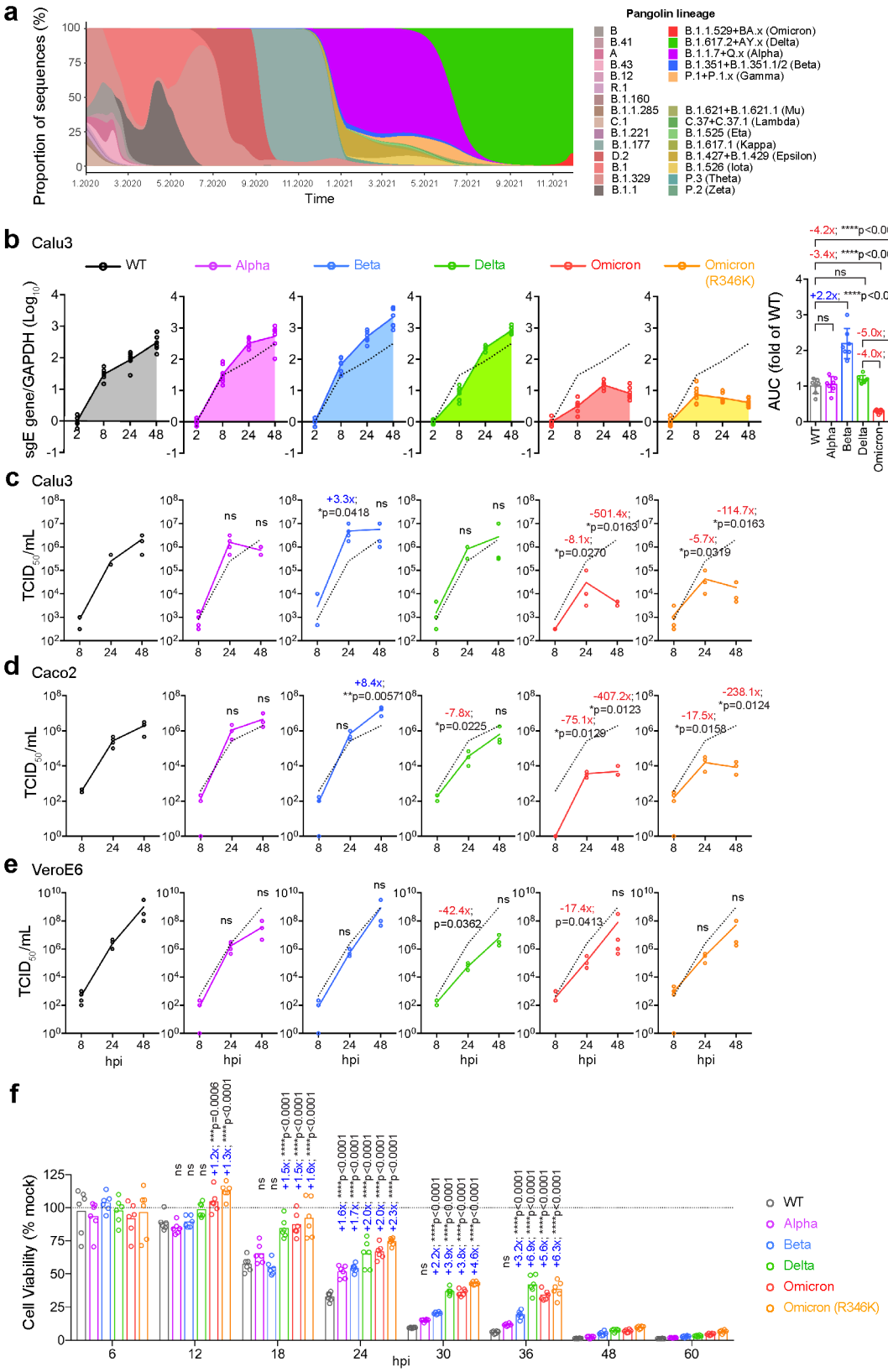

424

Fig. 1. Attenuated virus replication of SARS-CoV-2 Omicron. a The change in proportion of SARS-CoV-2 lineages deposited in GISAID from January 2020 to November 2021. The x-axis indicated collection date. The y-axis indicated the proportion of the selected SARS-CoV-2 lineages. **b-e** Cells were challenged with WT SARS-CoV-2 or Alpha, Beta, Delta, Omicron, or Omicron (R346K) at 0.5 MOI (for Calu3) or 0.1 MOI (for $CaCO_2$ and VeroE6). (b) Cell lysates and supernatants were harvested at designated time points for quantification of the subgenomic RNA of the envelope (sgE) gene (n = 7). Robustness of sgE production was quantified with the area under the curve (AUC) analysis. (c-e) Infectious viral particles were titrated with TCID50 assay (n = 4). **f** Cell viability of VeroE6-TMPRSS2 infected with WT SARS-CoV-2 and other variants at 0.1 MOI was quantified at the designated time points (n = 6). Data represents mean ± SD from the indicated number of biological repeats. Statistical significances were determined with one way-ANOVA in (b), Student's t-test in (c-e), or two way-ANOVA in (f). * represented $p < 0.05$ and ** represented $p < 0.01$. *** represented $p < 0.001$, **** represented $p < 0.0001$. ns, not statistically significant; WT, wildtype SARS-CoV-2.

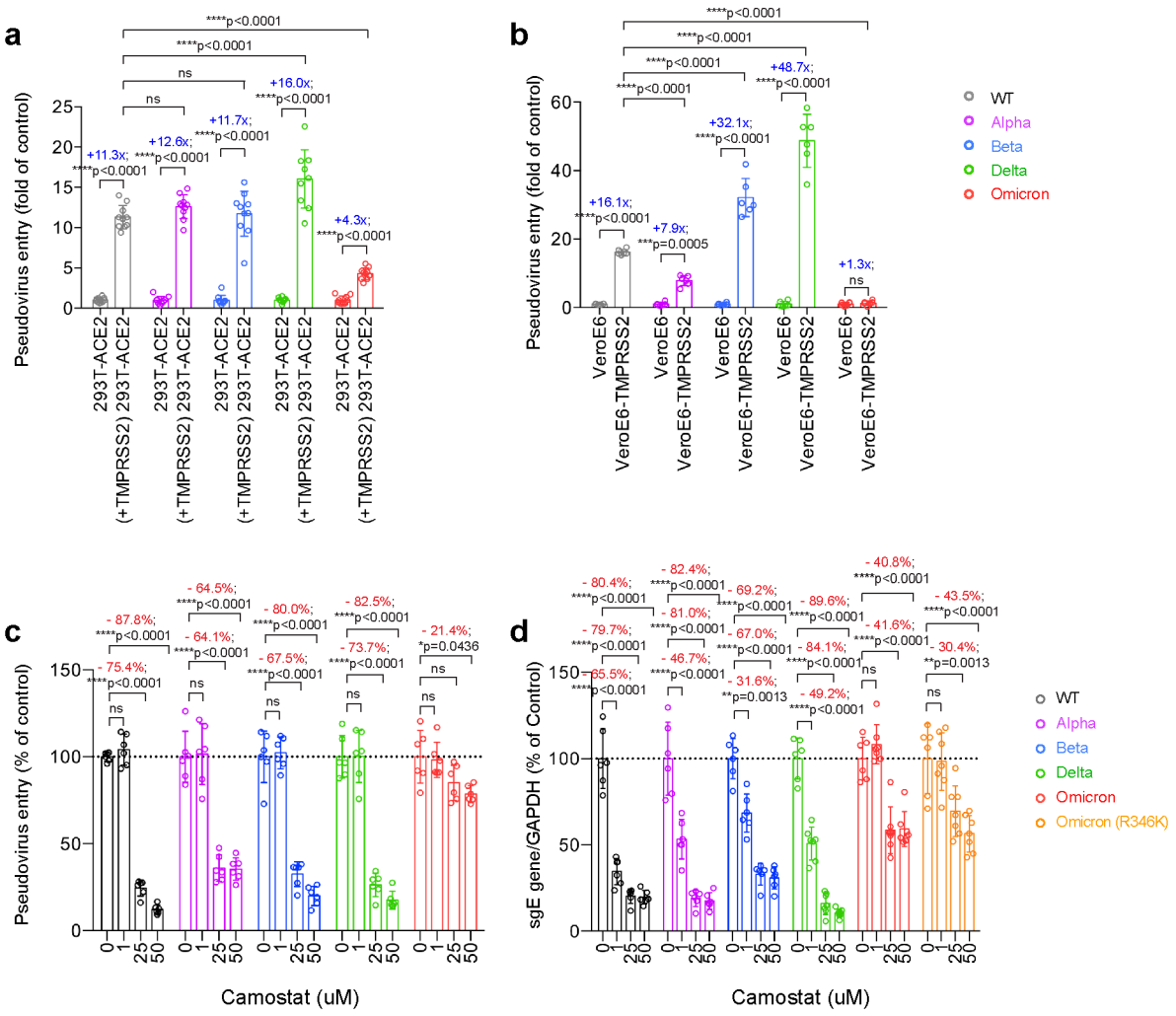

441

442 **Fig. 2. SARS-CoV-2 Omicron is deficient in TMPRSS2 usage. a** 293T cells were transfected
443 with ACE2 or co-transfected with ACE2 and TMPRSS2, followed by transduction with
444 pseudoviruses expressing the spike of WT SARS-CoV-2, Alpha, Beta, Delta, or Omicron variant
445 at 24 hours post transfection. Pseudovirus entry was quantified by measuring the luciferase
446 signal of the cell lysates at 24 hours post transduction (n = 10). Fold changes in the luciferase
447 signal was normalized to the mean luciferase readouts of cells with only ACE2 overexpression. **b**
448 VeroE6 and VeroE6-TMPRSS2 cells were transduced with pseudoviruses expressing the spike
449 of WT SARS-CoV-2, Alpha, Beta, Delta, or Omicron variant. Pseudovirus entry was quantified
450 by measuring the luciferase signal of the cell lysates at 24 hours post transduction (n = 6). **c-d**

VeroE6-TMPRSS2 cells were pre-treated with 1, 25, or 50μM camostat or DMSO for 2 h at 37 °C. The pre-treated cells were transduced with pseudoviruses expressing the spike of WT SARS-CoV-2, Alpha, Beta, Delta, or Omicron variant (c) or challenged with the indicated authentic SARS-CoV-2 variants at 0.1 MOI for 2h at 37 °C (d). Pseudoviruses entry was quantified by measuring the luciferase signal of the cell lysates at 24 hours post transduction (n=6). The amount of viral subgenomic envelope RNA in harvested cell lysate samples at 24hpi was determined by qRT-PCR (n=6). Data represents mean ± SD from the indicated number of biological repeats. Statistical significance was determined with two way-ANOVA (a-d). * represented $p < 0.05$ and ** represented $p < 0.01$. *** represented $p < 0.001$, **** represented $p < 0.0001$. ns, not statistically significant. WT, wildtype SARS-CoV-2.

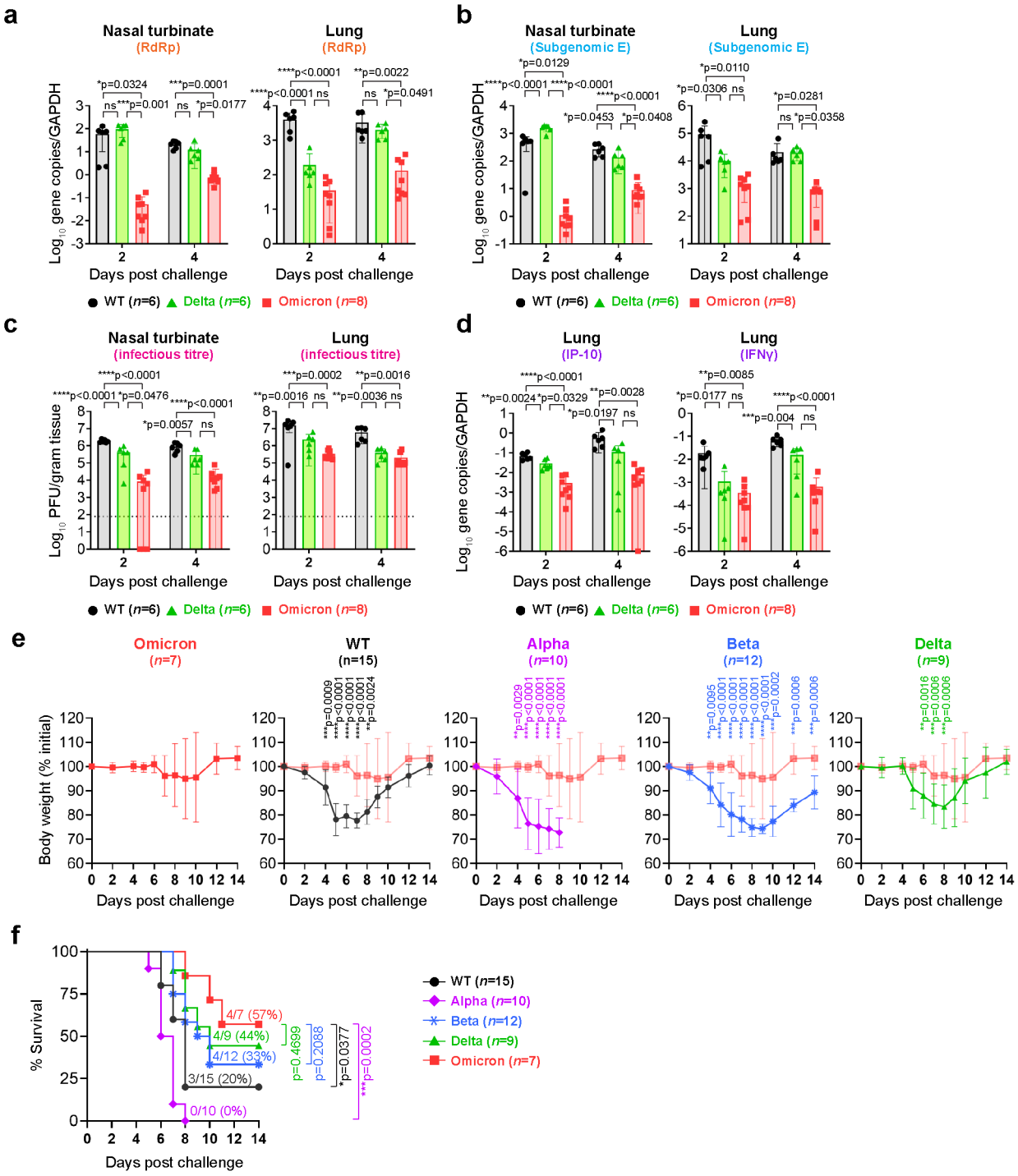

461

462 **Fig. 3. Attenuated replication and pathogenesis of Omicron in K18-hACE2 transgenic**

463 **mice.** 6-to-8-week-old female and male K18-hACE2 transgenic mice were intranasally

464 inoculated with 2×10^3 PFU Alpha, Beta, Delta, Omicron or WT SARS-CoV-2. Nasal turbinate

465 and lung of the infected mice were collected on 2 or 4 dpi for viral burden determination (n = 6-

8). Body weight and survival of the infected mice were monitored for 14 days (n = 7-15). **a** Viral RNA-dependent RNA polymerase (RdRp) gene copies were quantified with probe-specific RT-qPCR. **b** Subgenomic envelope (E) gene expression was quantified with probe-specific RT-qPCR. **c** Infectious viral titers were quantified with plaque assay in VeroE6-TMPRSS2 cells. **d** Inflammatory cytokines IP-10 and IFNγ were quantified with RT-qPCR. **e-f** Body weight and survival of the mice infected with WT SARS-CoV-2, Alpha, Beta, Delta, or Omicron variants. Data represents mean ± SD from the indicated number of biological repeats. Statistical differences were determined with one-way analysis of variance (ANOVA) in (a-d), Student's t-test in (e) or Log-rank (Mantel-Cox) test in (f). * represented $P < 0.05$; ** represented $P < 0.01$; *** represented $P < 0.001$; **** represented $P < 0.0001$. ns, not statistically significant; WT, wildtype SARS-CoV-2.

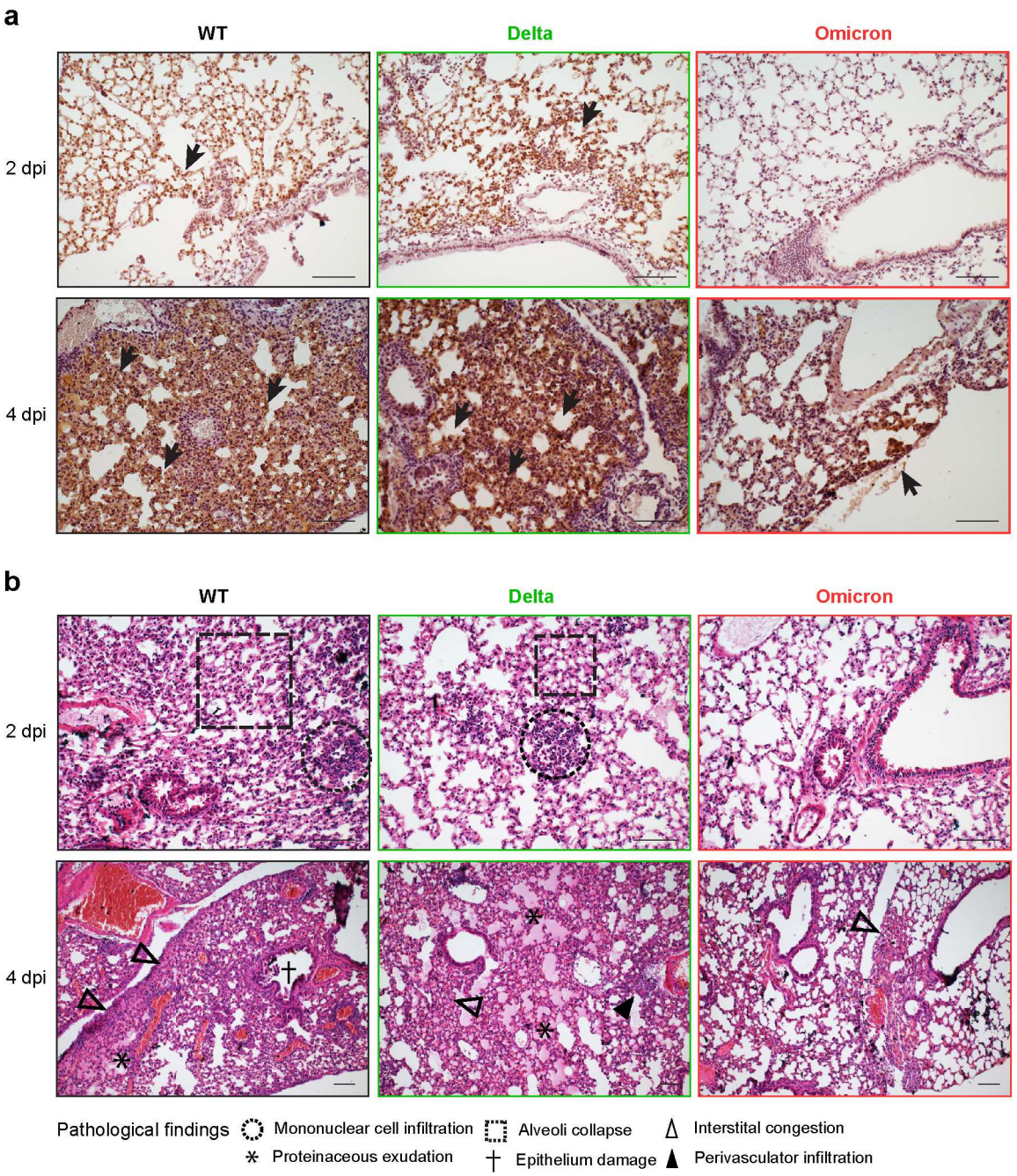

Fig. 4. Reduced in vivo pathology induced by Omicron infection. 6-to-8-week-old female and male K18-hACE2 transgenic mice were intranasally inoculated with 2×10^3 PFU Alpha, Beta, Delta, Omicron, or WT SARS-CoV-2. Lung of the infected mice were collected on 2 or 4 dpi for histological analysis. **a** Representative images of immunohistochemistry staining for the detection of nucleocapsid protein (brown, pointed by black arrows) of SARS-CoV-2 in lung of

the infected mice. **b** Representative images of hematoxylin and eosin (H&E) staining for the detection of pathological tissue damage in the lung of the infected mice. Images in (a and b) are representative images from three to four mice. Four to six sections were taken from each mouse for histology and immunochemistry analysis. Scale bar represents 200 μm. WT, wildtype SARS-CoV-2.

Methods

Viruses and safety

Wild type SARS-CoV-2 HKU-001a (GenBank accession number MT230904), B.1.1.7/Alpha (GISAID: EPI_ISL_1273444), B.1.351/Beta (GISAID: EPI_ISL_2423556), B.1.617.2/Delta (GISAID: EPI_ISL_3221329), B.1.1.529/Omicron (GISAID accession number EPI_ISL_7138045) and B.1.1.529/Omicron (R346K) (GISAID accession number EPI_ISL_7357684) were isolated from laboratory-confirmed COVID-19 patients in Hong Kong. All variants of SARS-CoV-2 were cultured using VeroE6-TMPRSS2 cells and titrated by plaque assays. In vivo and in vitro experiments with infectious SARS-CoV-2 were performed according to the approved standard operating procedures of the Biosafety Level 3 facility at Department of Microbiology, HKU. Dynamic changes of variants were inferred from metadata downloaded from GISAID (https://www.gisaid.org/, downloaded on 2021.12.16). Sequences with assembled genome length less than 2900bp or non-human host sequence were removed. World Health Organization prompted variants of interest (VOI), variants of concern (VOC) lineages, or lineages with proportions exceeded 20% of all variant lineages in any single day during the pandemic were kept.

Cell cultures

Caco2, 293T, and VeroE6 were obtained from ATCC and maintained in Dulbecco's modified Eagle's medium (DMEM) (Gibco, Amarillo, Texas, USA) according to supplier's instructions. Calu3 was obtained from ATCC and maintained in DMEM/F12 (Gibco). VeroE6-TMPRSS2 was obtained from the Japanese Collection of Research Bioresources (JCRB) Cell Bank and cultured in DMEM. All cell lines used are routinely tested for mycoplasma and are maintained mycoplasma-free.

In vivo virus challenge in mice

The use of animals was approved by the Committee on the Use of Live Animals in Teaching and Research of The University of Hong Kong under CULATR #5440-20. Heterogenous K18-hACE2 C57BL/6J mice (2B6.Cg-Tg(K18-ACE2)2Prlmn/J) were obtained from The Jackson Laboratory. For virus challenge in mice, 6- to 8- week-old female C57BL/6J mice or K18-hACE2 transgenic mice were anaesthetized with ketamine and xylazine, followed by intranasal inoculation with 20 μl/mouse of Alpha, Beta, Delta or Omicron variants or WT SARS-CoV-2 at 2×10^3 PFU/mouse (for K18-hACE2 transgenic mice) or 1×10^5 PFU/mouse (for C57BL/6J mice) as we previously described [cite eBioMed paper]. Mice were sacrificed at 2 and 4 dpi for harvesting nasal turbinate and lung tissues for virological assessment, proinflammatory cytokine quantification, or histological examination. Survival and body weight of the infected animals were monitored for 14 days or until death of the animal.

Histology and immunohistochemistry staining

Animal tissues were harvested and fixed with 10% neutral-buffered formalin. Nasal turbinates were decalcified with 10% formic acid for 7 days before being processed with the TP1020 Leica semi-enclosed benchtop tissue processor. IHC was performed with the DAB (3,3'-diaminobenzidine) substrate kit (Vector Laboratories) as we previously described [cite Chu, Sci

Adv paper]. To detect the viral antigen, in-house mouse monoclonal biotinylated anti-SARS-CoV-2 nucleocapsid protein antibody was used, followed by color development with the DAB substrate kit. The nuclei were detected with haematoxylin before the tissue sections was mounted with the VectaMount permanent mounting medium (Vector Laboratories). For H&E staining, tissue sections were stained with Gill's haematoxylin and eosin-Y. Images were acquired with the Olympus BX53 light microscope. Three to four mice were sampled each group (as specified in the figure legends) and four to six sections from each animal were used for histology analysis.

Infectious virus titration by plaque assays

Organs harvested from infected mice were homogenized in DMEM with Tissue Lyzer II (Qiagen, Germany) and clarified supernatants were 10-fold serially diluted inoculated to monolayered VeroE6-TMPSS2 cells for 2h at 37°C. After inoculation, the cells were washed with PBS three times, and covered with 1% low-melting agarose DMEM containing 1% FBS. The cells were fixed by 4% paraformaldehyde after 72h incubation. Fixed samples were stained with 0.5% crystal violet in 25% ethanol/distilled water for plaque visualization.

Infectious virus titration by $TCID_{50}$ assays

Supernatants from cells infected with Alpha, Beta, Delta, Omicron variant or wildtype SARS-CoV-2 were harvested and performed 10-fold serial dilution before inoculation into VeroE6-TMPRSS2 cells with 4 replicates per sample. Cytopathic effect (CPE) was observed at 72 hpi for the quantification of the median tissue culture infectious dose.

Cell viability assays

VeroE6-TMPRSS2 cells were infected with Alpha, Beta, Delta, Omicron variant or wildtype SARS-CoV-2 at 0.1 MOI. Cell viability was quantified by CellTiter-Glo luminescent cell

viability assay kit (Promega, USA), following manufacturer's manual with a multilabel plate reader Multiscan FC (Thermo Fisher Scientific, USA) at the designated time points.

Production of SARS-CoV-2-Spike-pseudoviruses and pseudovirus entry assays

All variants of SARS-CoV-2-spike pseudoviruses were packaged as described previously. In brief, 293T cells were transfected with different spikes with Lipofectamine 3000 (Thermo Fisher Scientific, Waltham, MA, USA). At 24 h post transfection, the cells were transduced with VSV-deltaG-firefly pseudotyped with VSV-G. At 2 h post transduction, the cells were washed 3 times with PBS and cultured in fresh media with anti-VSV-G (8G5F11) antibody (EB0010, kerafast, Boston, MA, USA). The pseudoviruses were then harvested 16 hours post transduction and titrated with $TCID_{50}$. For pseudovirus entry assays, target cells were inoculated with pseudoviruses for 2h and cultured in 1% FBS media for 24 h, before washed and lysed for detection of luciferase signal with a luciferase assay system (E1501, Promega, Madison, WI, USA).

RNA extraction and real-time reverse-transcription polymerase chain reaction

Viral RNA from infected cells was extracted using QIAsymphony RNA Kit (931636, Qiagen, Germantown Road Germantown, MD, USA). Viral RNA from mice lung and nasal turbinate samples were extracted with the RNeasy Mini kit (74106, Qiagen). SARS-CoV-2 gene copies targeting the RNA-dependent RNA polymerase (RdRp) were quantified using the QuantiNova Probe RT-PCR Kit (208354, Qiagen). Viral subgenomic RNA was detected using primer targeting E gene. The expression of IP-10 and IFN-gamma were detected by qRT-PCR using the QuantiNova SYBR Green RT-PCR kit. The primer and probe sequences are listed in **Extended Data Table 1.**

Protease inhibitor treatment assay

The serine protease inhibitor, camostat, was purchased from MedChemExpress (Monmouth Junction, NJ, USA). VeroE6-TMPRSS2 cells were treated with camostat at concentrations of 1 ,25, and 50μM for 2 h before virus infection or pseudovirus transduction. At 24 hpi, the cell lysates were harvested for qRT-PCR quantification of virus replication or lysed for detection of luciferase signal.

Statistical analysis

Statistical comparison between two experiment groups were performed with unpaired Student's *t*-test. Comparison among three or more experiment groups was performed with one-way or two-way ANOVA with Tukey's multiple comparison test. Area under the curve were calculated and analyzed with one-way ANOVA. Survival of animals were compared with Log-rank (Mantel-Cox) test. Differences were considered statistically significant when $p<0.05$. Data analysis were performed with Graphpad prism 8.0.

Acknowledgments

Funding:

This work was partly supported by funding from the Health and Medical Research Fund (CID-HKU1-5, COVID1903010-14, and 20190652), the Food and Health Bureau, The Government of the Hong Kong Special Administrative Region; the General Research Fund (17118621) of Research Grants Council, The Government of the Hong Kong Special Administrative Region; Health@InnoHK, Innovation and Technology Commission, the Government of the Hong Kong Special Administrative Region; National Natural Science Foundation of China Excellent Young Scientists Fund (Hong Kong and Macau) (32122001); The University of Hong Kong Li Ka Shing Faculty of Medicine Enhanced New Staff Start-up Fund; National Program on Key

Research Project of China (grant no. 2020YFA0707500 and 2020YFA0707504); the Consultancy Service for Enhancing Laboratory Surveillance of Emerging Infectious Diseases and Research Capability on Antimicrobial Resistance for Department of Health of the Hong Kong Special Administrative Region Government, Sanming Project of Medicine in Shenzhen, China (No. SZSM201911014); the High Level-Hospital Program, Health Commission of Guangdong Province, China; the Major Science and Technology Program of Hainan Province (ZDKJ202003); the research project of Hainan academician innovation platform (YSPTZX202004); and the Hainan talent development project (SRC200003); and the donations of the Shaw Foundation Hong Kong, Richard Yu and Carol Yu, May Tam Mak Mei Yin, Michael Seak-Kan Tong, Lee Wan Keung Charity Foundation Limited, Hui Ming, Hui Hoy and Chow Sin Lan Charity Fund Limited, Chan Yin Chuen Memorial Charitable Foundation, Marina Man-Wai Lee, the Hong Kong Hainan Commercial Association South China Microbiology Research Fund, the Jessie & George Ho Charitable Foundation, Perfect Shape Medical Limited, Kai Chong Tong, Foo Oi Foundation Limited, Tse Kam Ming Laurence, Betty Hing-Chu Lee, Ping Cham So, and Lo Ying Shek Chi Wai Foundation. The funding sources had no role in the study design, data collection, analysis, interpretation, or writing of the report.

Author contributions:

Conceptualization: HS, JFWC, BH, YC, KYY, HC

Methodology: HS, BH, YC, TTTY, HC

Investigation: HS, BH, YC, TTTY, XH, CY, JCH, HL, JS, YL, TZ, YH, JPC, AJZ, JZ, SY, BZZ, JDH

Visualization: HS, BH, YC, HC

Funding acquisition: JFWC, FY, KYY, HC

Project administration: JFWC, KYY, HC

Supervision: JFWC, KYY, HC

Writing – original draft: HS, JFWC, BH, YC, KYY, HC

Writing – review & editing: HS, JFWC, BH, YC, KYY, HC

Competing interests:

The authors declare no competing interests.

Data and materials availability:

Correspondence and requests for materials should be addressed to Hin Chu and Kwok-Yung Yuen.

Supplementary Information:

Supplementary information is available for this paper.

Extended Data Fig. 1. Virus replication of Omicron, WT SARS-CoV-2, and other VOCs in Caco2 and VeroE6 cells.

Extended Data Fig. 2. Omicron infection in C57B6 wildtype mice.

Extended Data Fig. 3. Body weight comparison between different VoCs and wildtype SARS-CoV-2.

Extended Data Fig. 4. Immunohistochemistry staining of lung tissue of K18-hACE2 transgenic mice infected with WT SARS-CoV-2, Delta, or Omicron variant.

Extended Data Fig. 5. H&E images of lung tissue of K18-hACE2 transgenic mice infected with WT SARS-CoV-2, Delta, or Omicron variant.

Extended Data Table. 1. Primer and probe sequences used for RT.

Extended data figures and figure legends:

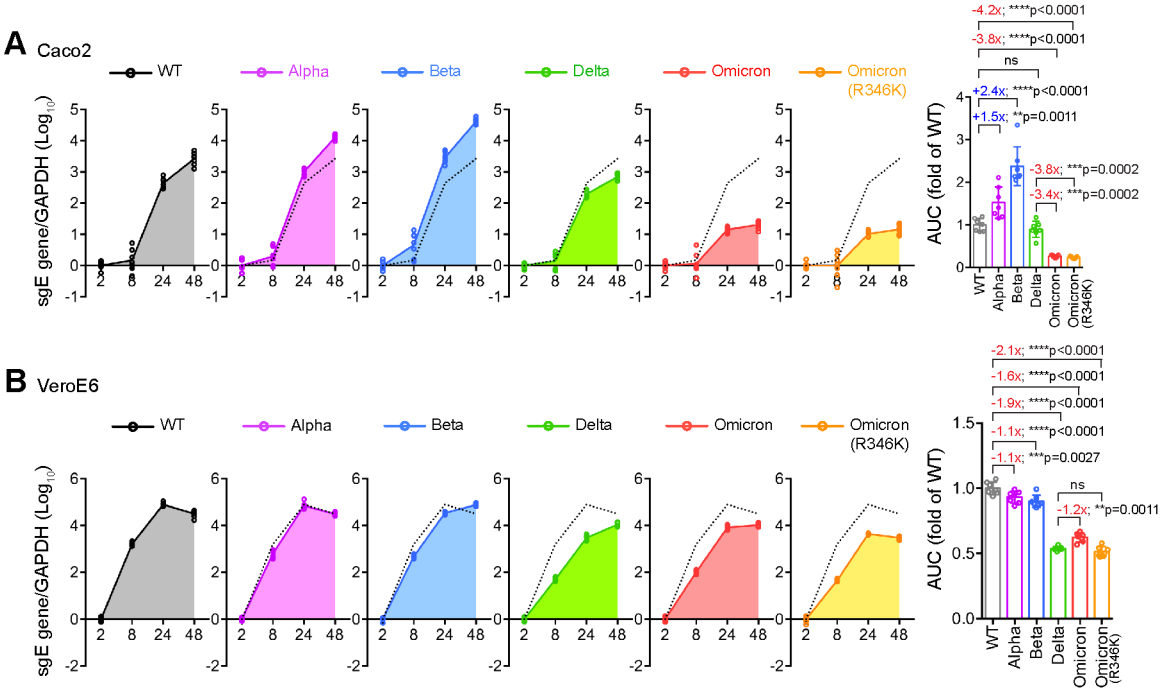

Extended Data Fig. 1. Virus replication of Omicron, WT SARS-CoV-2, and other VOCs in Caco2 and VeroE6 cells. (**A**) Caco2 and (**B**) VeroE6 cells were challenged by WT SARS-CoV-2, Alpha, Beta, Delta, Omicron, or Omicron (R346K) at 0.1 MOI. (**A**) Cell lysates were harvested at the designated time points for the quantification of subgenomic RNA of the envelope (sgE) gene. Robustness of sgE production was quantified with the area under the curve (AUC) analysis (n = 7). Data represents mean ± SD from the indicated number of biological repeats. Statistical significances were determined with one way-ANOVA in (A-B). * represented $p < 0.05$ and ** represented $p < 0.01$. *** represented $p < 0.001$, **** represented $p < 0.0001$. ns, not statistically significant; WT, wildtype SARS-CoV-2.

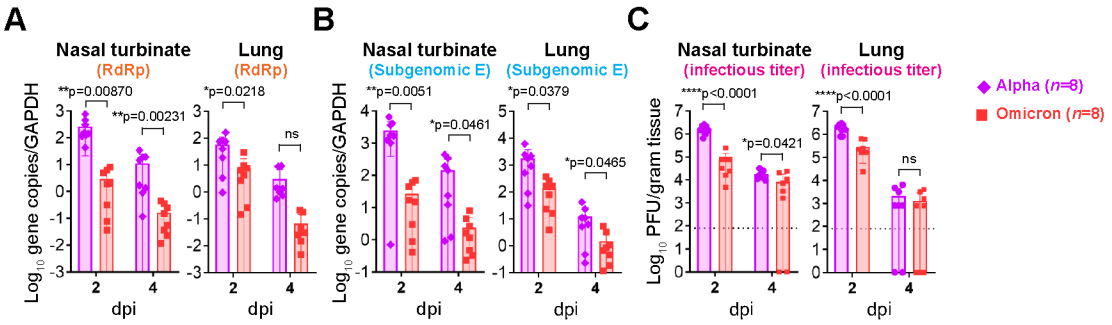

Extended Data Fig. 2. Omicron infection in C57B6 wildtype mice. 6-to-8-week-old female C57b6 wildtype mice were intranasally inoculated with 1×10^5 PFU of Alpha or Omicron variant. Nasal turbinate and lung of the infected mice were collected on 2 or 4 dpi. for viral burden determination (n = 8). (**A**) Viral RNA-dependent RNA polymerase (RdRp) gene copies were quantified with probe-specific RT-qPCR. (**B**) Subgenomic envelope (E) gene were quantified with probe-specific RT-qPCR. (**C**) Infectious viral titres were quantified with plaque assay in VeroE6-TMPRSS2 cells. Data represents mean ± SD from the indicated number of biological repeats. Statistical differences were determined with Student's t-test in (A-C). * represented $P < 0.05$; ** represented $P < 0.01$; *** represented $P < 0.001$; **** represented $P < 0.0001$.

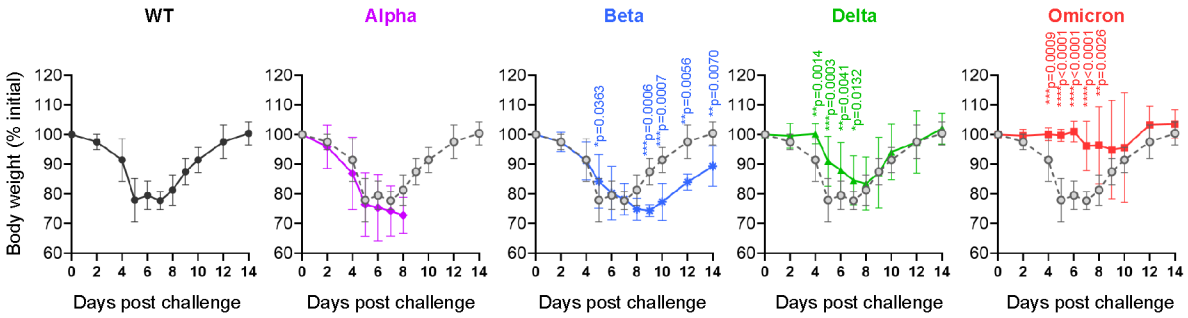

668

669 **Extended Data Fig. 3. Body weight comparison between different VOCs and wildtype**
670 **SARS-CoV-2.** 6-to-8-week-old female and male K18-hACE2 transgenic mice were intranasally
671 inoculated with 2×10^3 PFU or WT SARS-CoV-2, Alpha, Beta, Delta, or Omicron. Body weight
672 of the infected mice were monitored for 14 days (n = 7-15). Data represents mean ± SD from the
673 indicated number of biological repeats. Statistical differences were determined with Student's t-
674 test. * represented $P < 0.05$; ** represented $P < 0.01$; *** represented $P < 0.001$; ****
675 represented $P < 0.0001$.

676

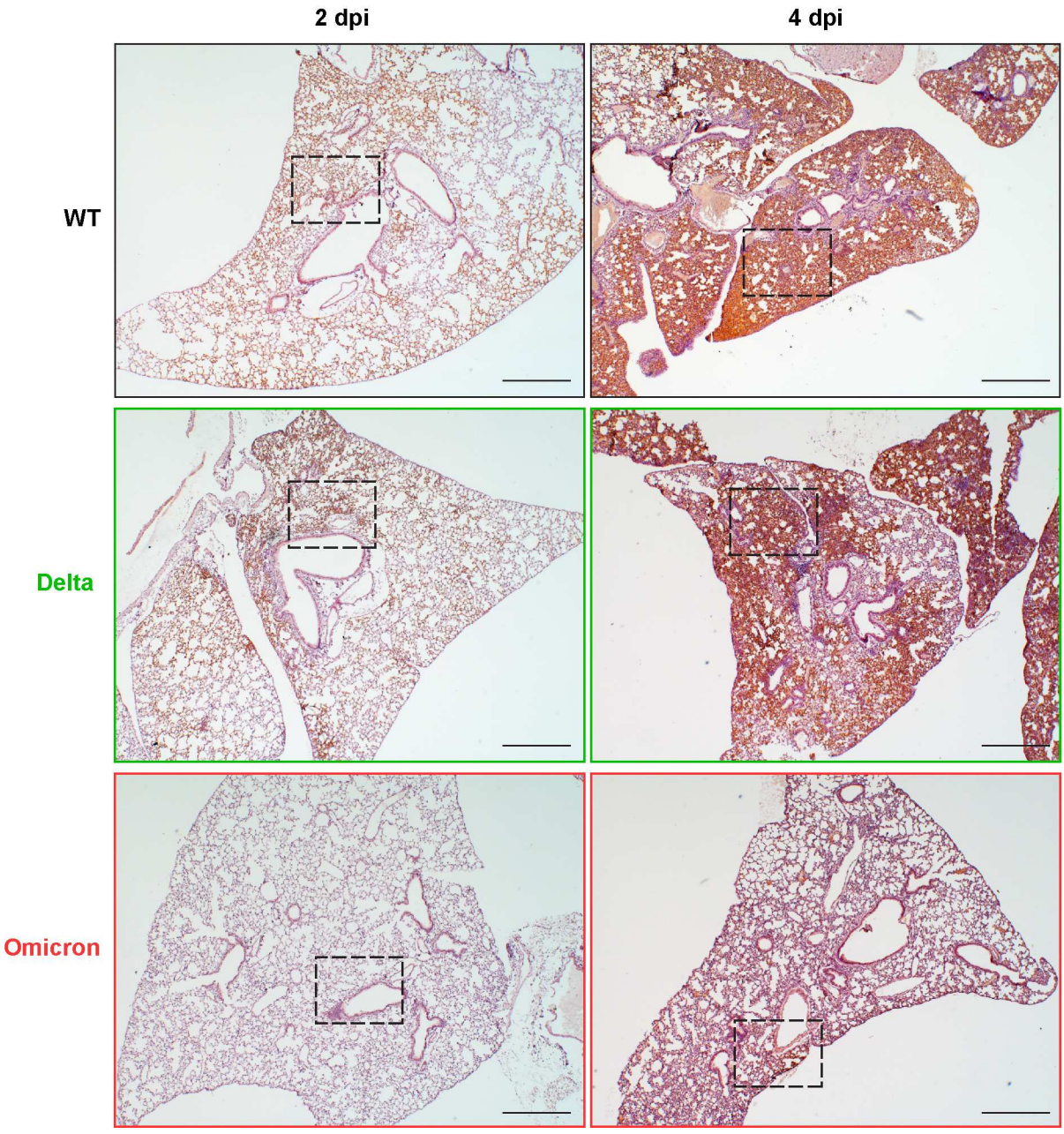

Extended Data Fig. 4. Immunohistochemistry staining of lung tissue of K18-hACE2 transgenic mice infected with WT SARS-CoV-2, Delta, or Omicron variant. 6-to-8-week-old female and male K18-hACE2 transgenic mice were intranasally inoculated with 2×10^3 PFU or WT SARS-CoV-2, Delta, or Omicron variant. Lung of the infected mice were collected on 2 or 4 dpi for histological analysis. Representative images of immunohistochemistry staining for the detection of nucleocapsid protein (brown, pointed by black arrows) of SARS-CoV-2 in lung of

684 the infected mice. Images are the source images with lower magnification for Figure 4A. Dashed
685 rectangles indicate the region enlarged in Figure 4A. Four to six sections were taken from each
686 mouse for histology and immunochemistry analysis. Scale bar represents 500 μm.
687
688

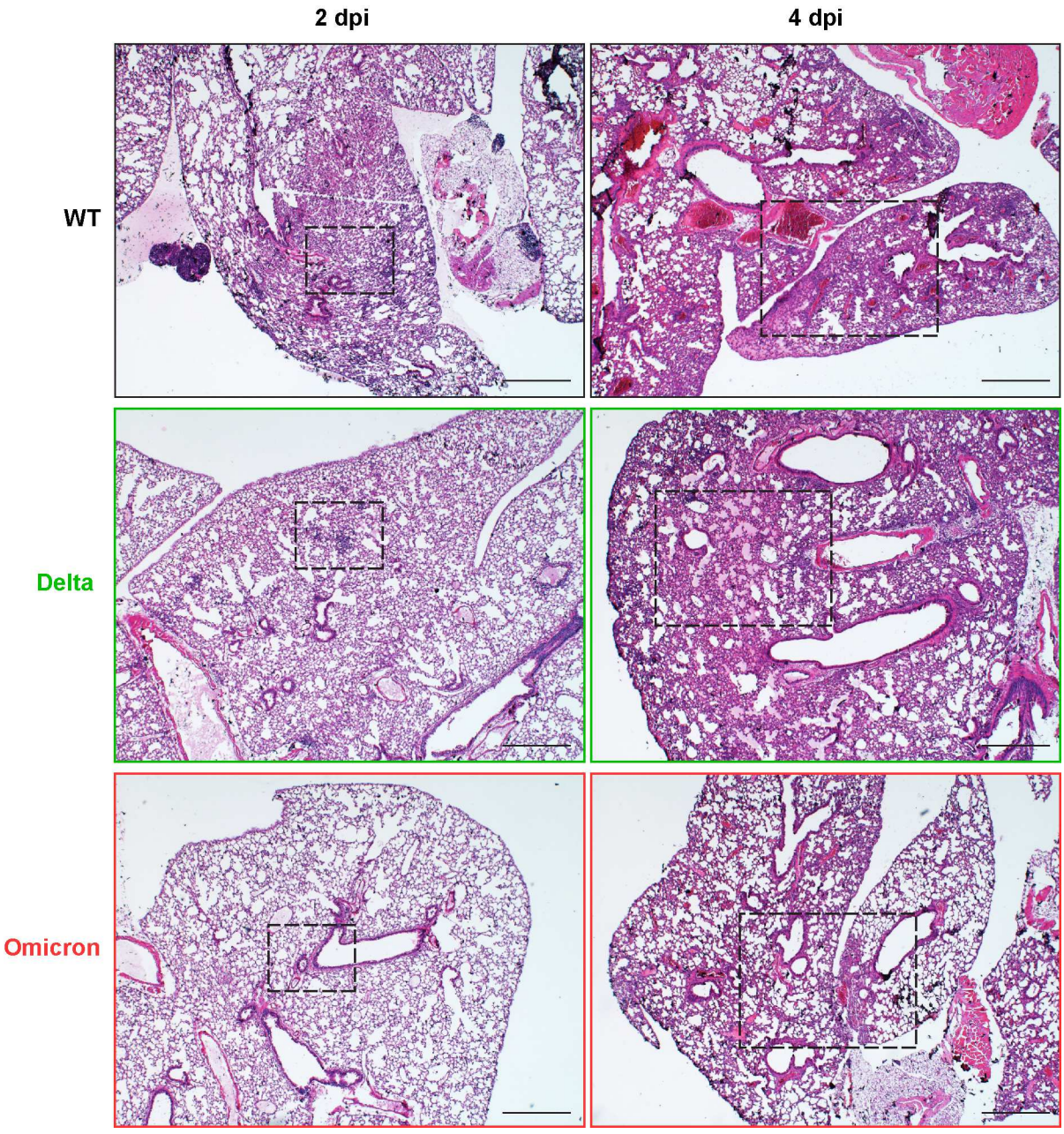

Extended Data Fig. 5. H&E images of lung tissue of K18-hACE2 transgenic mice infected with WT SARS-CoV-2, Delta, or Omicron variant. 6-to-8-week-old female and male K18-hACE2 transgenic mice were intranasally inoculated with 2×10^3 PFU WT SARS-CoV-2, Delta or Omicron variant. Lung of the infected mice were collected at 2 or 4 dpi for histological analysis. Representative images of hematoxylin and eosin (H&E) staining for the detection of pathological tissue damage in the nasal turbinate and lung of the infected mice. Images are the

source images with lower magnification for Figure 4B. Dashed rectangles indicate the region enlarged in Figure 4B. Four to six sections were taken from each mouse for histology and immunochemistry analysis. Scale bar represents 500 μm.

Extended Data Table 1. Primer sequences used for RT-qPCR in the current study.

Species	Gene	Sequence
SARS-CoV-2	RdRp	(F) 5'- CGCATACAGTCTTRCAGGCT -3' (R) 5'- GTGTGATGTTGAWATGACATGGTC -3' (probe) 5'- /FAM/TTAAGATGTGGTGCTTGCATACGTAGAC -/lABkFQ/3'
	subgenomic E	(F) 5'- CGATCTCTTGTAGATCTGTTCTC -3' (R) 5'- ATATTGCAGCAGTACGCACACA -3' (probe) 5'- /FAM/ACACTAGCCATCCTTACTGCGCTTCG -/lABkFQ/3'
Mouse	IP-10	(F) 5'- TACGTCGGCCTATGGCTACT -3' (R) 5'- TTGGGGACTCTTGTCACTGG -3'
	IFN γ	(F) 5'- AAGCGTCATTGAATCACACC -3' (R) 5'- CGAATCAGCAGCGACTCCTT -3'
	GAPDH	(F) 5'- ACTCCACTCACGGCAAATTC -3' (R) 5'- TCTCCATGGTGGTGAAGACA -3'
Human	GAPDH	(F) 5'-ATTCCACCCATGGCAAATTC-3' (R) 5'-CGCTCCTGGAAGATGGTGAT-3'

Supplementary Files

This is a list of supplementary files associated with this preprint. Click to download.

- FigureS1replicationofothercells1223.tif
- FigureS2SupplementaryfigureoimcronC57mice.tif
- FigureS3Supplementarybodyweight.tif
- FigureS4SupplementaryIHC.tif
- FigureS5SupplementaryHXE.tif